Qualitative Study on Electrolytic Decomposition of Hydroxylammonium Nitrate (HAN) Solution in PDMS-based Micro-combustion Chambers

Jitkai Chin, Kai Seng Koh* and Tengku Farah Wahida Ku Chik***
**University of Nottingham Malaysia Campus*
Jalan Broga, Semenyih 43500, Selangor, Malaysia
***Propulsion Division, National Space Agency (ANGKASA)*
Second Author's Address

Abstract
Although the decomposition mechanism has been demonstrated and studied in custom-made micro-combustion or micropropulsion systems, visualisation on the phenomenon inside micro-combustion chamber has never been reported. In this paper, Electrolytic decomposition of 73 wt% Hydroxylammonium Nitrate (HAN) solution was successfully demonstrated with DC power 300W in carefully designed transparent PDMS-based micro-combustion chambers. Experimental results show that more vigorous reaction occurred at high inlet flowrate of 50µl/min (Re = 0.88) in which only 10 – 48% of space inside the micro-combustion chamber occupied by the un-decomposed HAN solution compared to 40 – 62% at inlet flowrate of 10µl/min (Re = 0.18).

1. Introduction

Burning of HAN solution was first carried out in 1976, dedicated for liquid gun propellant development in which the burning rate of HAN solution was found to be inversely proportional to pressure increment in the combustion chamber [1]. In recent years, it is an attractive alternative for space researchers in attempt to replace conventional liquid monopropellant such as hydrazine and hydrogen peroxide (HTP) since it fulfils most of the critical criteria of a liquid monopropellant such as high density, low freezing point low viscosity, easier storage and non-toxic post-combustion species. With limited volume and weight to be carried up in the carrier, high energy density of HAN has shown compatible combustion performance compared to HTP and hydrazine at smaller amount of monopropellant required [2].

Conventional HAN solution combustion techniques involves thermal heating or catalytic ignition [3-5]. By such combustion techniques, heat is generally transferred from a heat source directly into the solution to reach ignition. The process results in huge energy loss from ignition, which is particularly significant in microstructures due to large surface-to-volume ratio. In recent years, electrolytic decomposition of HAN solution has been targeted to replace the conventional methods because energy is directly deposited into the solution to initiate ignition, thus improving the overall combustion efficiency. For example, DC power of 1.35kW was reported to decompose HAN solution in a Low Temperature Co-fired Ceramic Technology (LCCT) with 150mN of thrust achieved [6]. In addition, AC voltage ranging from 80-140V also successfully decomposed a HAN ternary solution into various decomposition gases (NO_x , O_2, H_2O) [7].

Although electrolytic decomposition of HAN solution in microsystems has been reported, visualisation on decomposition phenomenon in the system remained absent in literature. Understanding the flow and chemical reaction phenomenon in micro-combustion chamber is important for increasing its efficiency as well as improving future engineering design. In this paper, electrolytic decomposition of HAN solution was demonstrated in micro-combustion chambers fabricated with Polydimethylsiloxane (PDMS), which is transparent that enable visualisation. Qualitative investigation of HAN decomposition in the micro-combustion chambers, under various inlet flowrate conditions was also reported. Although PDMS is known to have relatively low melting temperature at 200 ^{0}C, the devices still managed to survive the decomposition process [8].

2. Theory

In electrolytic decomposition of HAN solution, the reaction starts with electrolysis of water. At anode, Production of protons from Rxn1 promotes the following reaction:

$$(NH_3OH)^+NO_3^- + H^+ \rightarrow NH_3OH^+ + HNO_3 \quad (2)$$

Therefore, overall equation at anode:

$$H_2O(l) + 2(NH_3OH)^+NO_3^- \rightarrow \frac{1}{2}O_2 + 2NH_3OH^+ + 2HNO_3 + 2e^- \quad (3)$$

At cathode:

$$2NH_3OH^+ \mid 2e^- \; : \; 2NH_2OH \mid H_2 \quad (4)$$

Hence, the overall reaction is

$$H_2O + 2(NH_3OH)^+NO_3^- \rightarrow \frac{1}{2}O_2 + 2HNO_3 + 2NH_2OH + H_2 \quad (5)$$

In anode, the deficiency of proton filled up by excessive mobile proton from cathode (*Rxn4*) when power supply that acts as initiation tool for proton transfer process is cut off. Hence, the decomposition is able to take place continuously until the energy gain in the system is unable to cross the energy barrier required to trigger decomposition [7]. The overall reaction (*Rxn5*) is in line with the classic autocatalytic reactions of thermal decomposition HAN shown as below [9]:

$$HAN + H_2O \rightarrow NH_2OH + HNO_3 + H_2O \quad (6)$$

$$NH_2OH + HNO_3 \rightarrow HONO + HNO + H_2 \quad (7)$$

$$NH_2OH + HONO \longrightarrow N_2O + 2H_2O \quad (8)$$

$$NH_2OH + HNO \longrightarrow N_2 + 2H_2O \quad (9)$$

$$3HONO \longrightarrow 2NO + HNO_3 + H_2O \quad (10)$$

$$2HNO \longrightarrow N_2O + H_2O \quad (11)$$

$$HNO + HNO_3 \longrightarrow 2HONO \quad (12)$$

$$HONO + HNO_3 \longrightarrow 2NO_2 + H_2O \quad (13)$$

The induction period (*Rxn6*) is the rate determining step, which is greatly influenced by water content in the HAN solutions [7]. In this study, activation energies are used to predict the behaviour of each reaction in different stages of autocatalytic reactions. For instance, in decay stage, *Rxn 13* and *Rxn 8* consume HONO simultaneously. *Rxn 10* gives nitric acid as a product, which also acts as a reactant in the explosion stage (7). Therefore, *Rxn 8* will be more likely to occur compared to *Rxn 13*. For *Rxn 9* and *Rxn 10*, kinetic equations are not preferred as they involve a triple bond break down or formation of nitrogen atom, causes extra energy needed to overcome the energy barrier. The main products of thermal decomposition of HAN are nitrogen gas and water vapor (7). However, the entire combustion

mechanism such as residence time between reactions and the conversion rate of the chemical equations is still not fully understood, hence giving uncertainties in analysing the overall decomposition process.

3. Experiment

3.1 Synthesis of HAN solution

HAN solution was prepared by titration between aqueous solution of hydroxylamine (50 wt%) and nitric acid (35 wt%), both of high purity (Sigma-Aldrich). The process was continuously kept in ice water bath to avoid self-decomposition until pH of the solution reached 2.50. The pristine solution was then further purified in a rotary evaporator (Heidolph Laborota 4003) for 19 minutes to achieve approximately 73 wt% HAN solution. By using conventional volume and weight measurement method, the density of the HAN solution is 1.524 g/cm^3 while viscosity of the solution at room temperature is 9.0×10^{-4} PaS (LVDV-II Viscometer, Brookfield).

3.2 Fabrication of micro-combustion chambers

The micro-combustion system consists of a reservoir as shown in the left in Figure 1, a microchannel connecting the reservoir to micro-combustion chamber located at the right of the figure. The design was fabricated using xurographic method, in which the pattern was firstly cut into shape on a vinyl film using a cutting plotter (Graphtec CE5000-60), followed by fabrication steps illustrated in Figure 2. After the device was completed, copper wires were directly poked through the PDMS top layer into the micro-combustion chamber to serve as electrodes, as shown in Figure 3.

Our previous study has shown that macroscale HAN solution decomposition behaviour was influenced by electrodes selection [10]. Sacrificial electrodes such as copper wire may generate more reactive chemical reaction compared to inert electrodes.

Three devices were fabricated to study decomposition phenomenon under different flowrates in each micro-combustion chamber. The positions of copper wire electrodes varied slightly even though best effort was put in to ensure consistency. The distances between electrodes in Devices A, B and C were 1.37mm, 0.42mm and 0.98mm respectively. The distances between electrodes at this scale (<5 mm) has negligible influence on the efficiency of electrolytic decomposition [11].

Figure 1: Device pattern on a vinyl film. The circle at the left of the mask indicates the reservoir (5mm radius × 200 µm (H)), connecting to the micro-combustion chamber (2mm (W) × 3mm (L) × 200 µm (H)) via a serpentine microchannel (225µm (W) × 15mm (L) × 200 µm (H)), which will avoid HAN solution backflow due to high pressure in the micro-combustion chamber. The extra markers (1 mm (W) × 1mm (L) × 200 µm (H)) next to the chamber were used as mark for insertion of copper wire. Post combustion products were released from the combustion chamber into the ambient in the right.

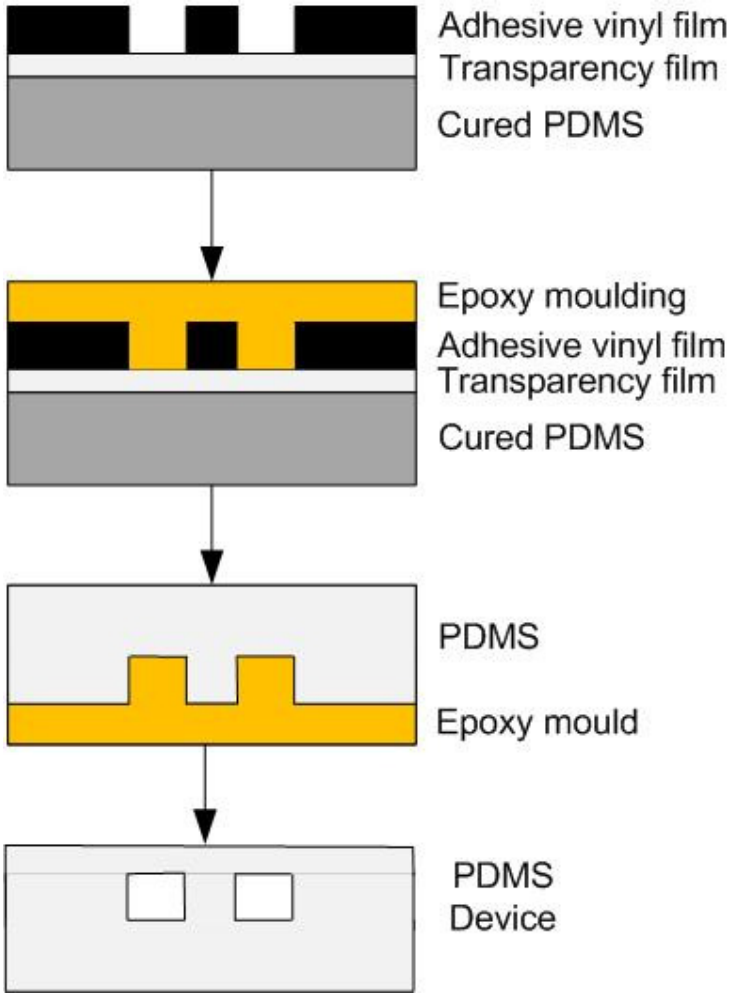

Figure 2: Fabrication of the micro-combustion device. A) The undesired vinyl film was peeled off to create a negative mould attached to a transparent transfer film before it was attached to a PDMS slab to form a mould for the entire microstructure, to encase the poured PDMS mixture. B) Mixture of Bisphenol A (BPA) was poured onto the mould, then cured naturally at room temperature for 48 hours. C) PDMS poured onto the epoxy mold and allowed to dry naturally. D) The channels were formed by sealing it with a PDMS top piece with Piranha solution, followed by thermal curing at $70\,^{0}$C for 60 minutes [11].

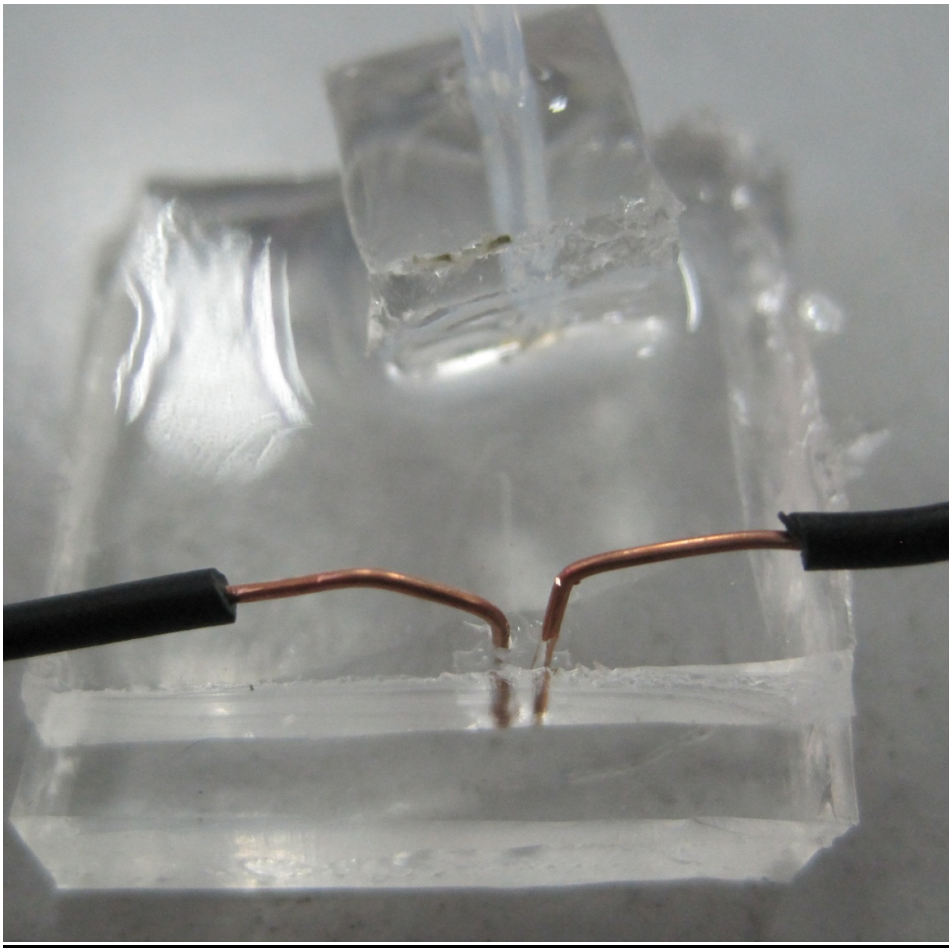

Figure 3: System A with copper wires directly poked into it used as microelectrodes.

Before experiment, the devices were primed with the HAN solution, delivered into the reservoirs through 1/16" PTFE tube (Omnifit) driven by a syringe pump (KDS 210, KDS Scientific), to ensure no air bubbles trapped in the devices. 300W of DC power supply (PS 8040-120 2U, Elektro-Automatik) connected to the copper microelectrodes switched on with the HAN solution continuously fed into the devices. The decomposition lasted for 30 seconds, observed under a light inverted microscope (Olympus IX51) and recorded with a digital camera (Infinity Lite, Lumenera Corp.). The videos taken were processed and splitted into individual pictures (SC Video Cut and Split) for void analysis. Experiment in each device was repeated twice before the bonding finally failed. A video of experiment at Re = 0.18 is attached.

Several assumptions were made to facilitate the study. First, the diameter and surface of copper wires were identical in all experiments. Also, all gas bubbles generated in the micro-combustion chambers were only due to decomposition of HAN solution. In addition, in order to facilitate calculation of void fraction in the micro-combustion chamber, gas phase was assumed to be limited by the height of the chamber, like a pancake shape.

4. Results and discussions

Figures 4 are series of pictures extracted from videos taken during decomposition of HAN solution in different micro-combustion devices. The dimensions were identical as outlined in green line in Figure 4a. While distance between each pair of electrodes in the devices varied since the copper wires were directly poked into the devices. HAN solution was delivered from upstream reservoir in the left, undergo decomposition in the chamber, followed by displacement into ambient in the right.

Re = 0.18 (Flowrate = 10 µl/min) (Device A)	*Re* = 0.53 Flowrate = 30 µl/min (Device B)	*Re* = 0.88 Flowrate = 50 µl/min (Device C)
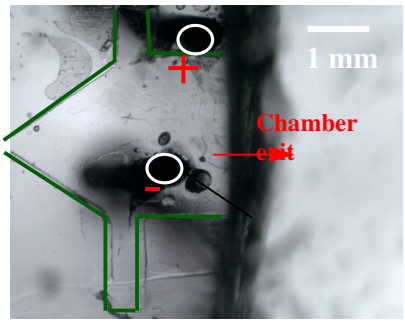 (a) t= 0 s	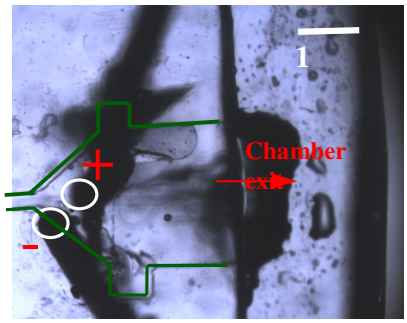 (g) t= 0 s	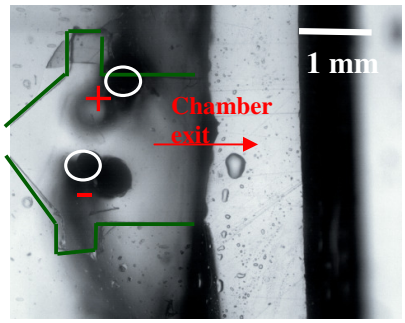 (m) t= 0 s
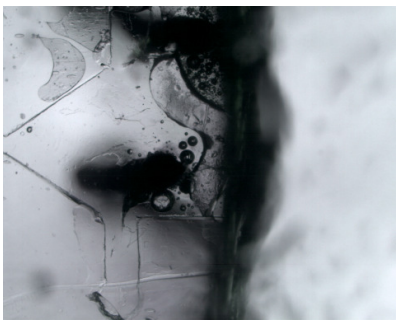 (b) t= 1.71 s	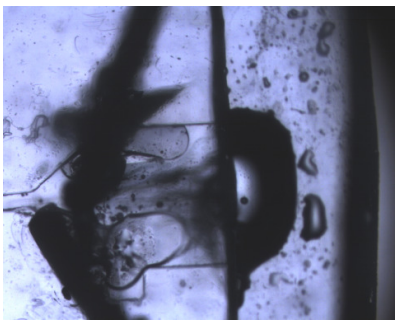 (h) t= 1.71 s	 (n) t= 1.71 s
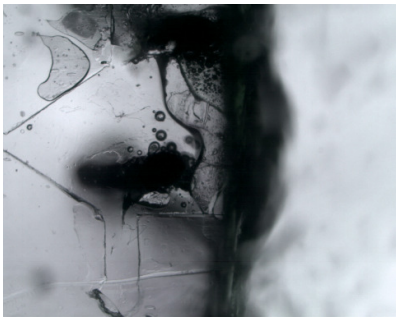 (c) t= 4.71 s	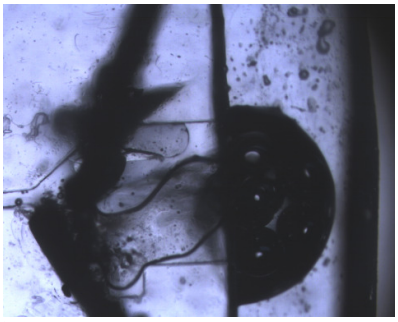 (i) t= 4.71 s	 (o) t= 4.71 s
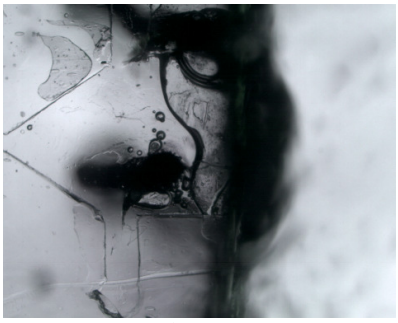 (d) t= 8.62 s	 (j) t= 8.62 s	 (p) t= 8.62 s

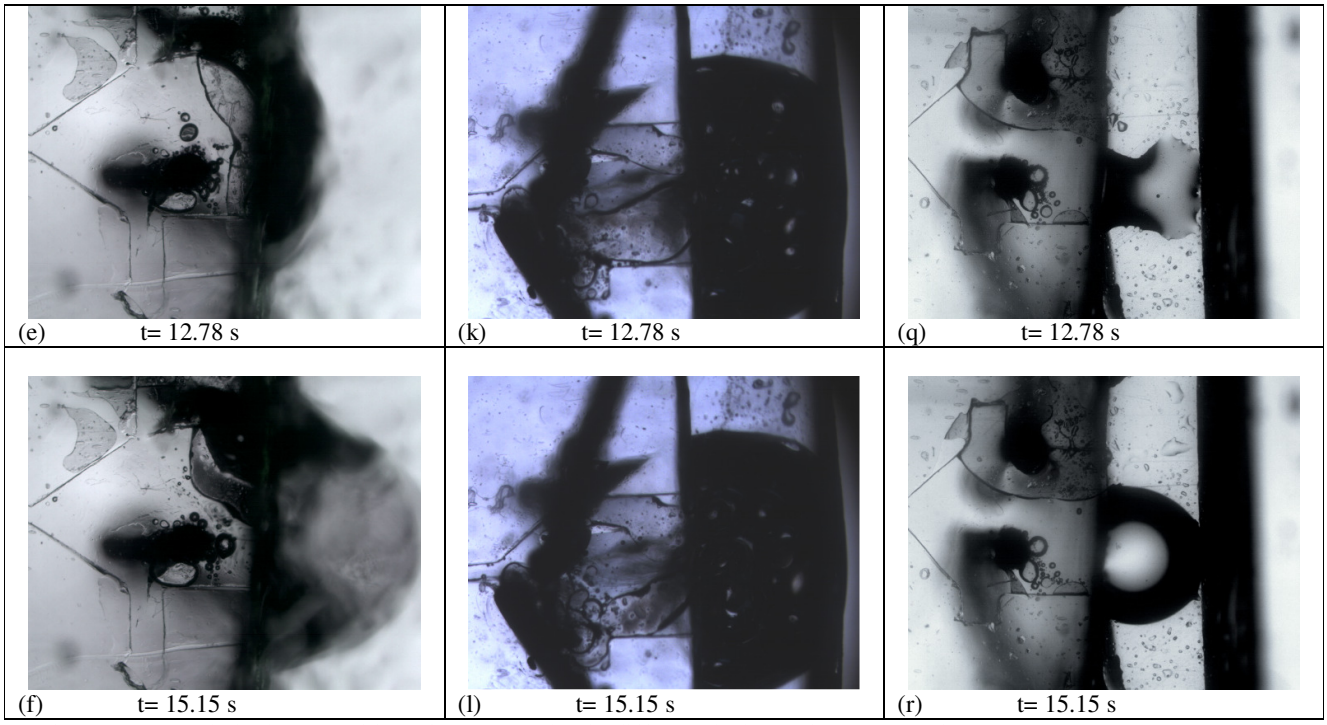

Figure 4: Electrolytic decomposition of HAN solution in different devices using copper wire

When when power was switched on (Figure 8b) while Device A was fed with inlet flowrate of 10µl/min or *Re* = 0.18, gas bubbles of oxygen and hydrogen, diameter in the range of 50 - 480µm were formed immediately at anode and cathode respectively, with the formation of bubbles at anode was milder than the cathode. Coalescence of bubbles took place before they were displaced to the chamber exit. Wave of decomposition with an interval of 0.92 second was observed with continuous yet consistent full combustion waves with time interval deviation less than 5% was recorded throughout whole experiment (Figure 8b – f).

Low *Re* preventing gas bubbles displaced to the ambient immediately after decomposition, due to significant wall effect. Some were stagnant almost throughout the decomposition process, resulted in choking at the exit (Figure 8d – f). The formation of void by trapped gas caused significant problem to the decomposition in the micro-chamber. Increase in void fraction causes increase in electrical resistance between the electrodes, even breakdown of electrical circuit (Figure 8e, f), resulting in decrease of efficiency. However, the circuit can still be completed through HAN solution accumulated at the chamber exit. In this circumstance, small air bubbles continuously formed at the electrodes as decomposition took place in random pattern both spatially and temporally in the chamber. The processes caused the void inside the micro-combustion chamber varied from 38 – 60%. Besides, no brownish post-combustion gases were noticed throughout experiment as the decomposition became more vigorous with post-combustion gas propagate to the exit.

In Device B, experiment was repeated at *Re* = 0.53. The decomposition phenomenon could be divided into two main visible stages, i.e. the transient and steady decomposition stage. In the transient stage, vigorous and continuous bubbles formation took place at both electrodes that the interval delay between bubble formation reduced from 0.55s down to 0.31s (Figure 8g) before it moved into the steady stage, in which the decomposition behaved more vigorous and propagated towards the chamber exit as continuous growth in two phases flow from t = 4.02s until t = 12.78s (Figure 8i – k). In this stage, time required between bubbles formation at the chamber exit continuously reduced. In addition, gas released from the reaction was significant that occupying 45 – 75% of space in the chamber, causes the wall effect becomes insignificant (Figure 8l). In general, the flow phenomenon in the chamber was more completed with rapid and random formation of large bubbles at the chamber exit.

In Device C, when the flowrate was further increased to 50µl/min, at *Re* = 0.88, consistent decomposition interval of 0.5s was noticed for the first 4.5s before the overall process was shortened to 0.2s after a few cycles (Figure 8m – p). The overall decomposition was more rigorous that only few small bubbles formed at the surroundings of electrodes while two phases flow in the chamber is smooth without serious problem of choking the exit. By contrast, space

inside the chamber was mostly occupied by gas generated throughout the duration, typically in the range of 58 – 90% (Figure 8p, q). Accumulation of HAN solution in the chamber also shortened significantly because of the relatively high flowrate.

Although flow and chemical reaction phenomenon in the micro-combustion chambers behaved differently as *Re* increased, no reverse flow into the upstream microchannel was observed in all devices. In addition, the chemical reaction, which was considered highly energetic, caused only slight de-sealing at the surroundings near to the chamber in all devices. However, the devices failed completely after experiments were repeated.

5. Conclusions

Although PDMS is not the ideal material for constructing micro-combustion system due to its relatively low melting point, it still enabled visualisation of microscale decomposition of HAN solution, which has never been reported in literature elsewhere. The micro-combustion systems were only effective in relatively high *Re* in which choking was reduced significantly. In addition, un-decomposed HAN solution in the micro-combustion chambers is the main concern in future engineering design as it caused complex two phase flow which is difficult to predict and reducing efficiency of the devices. The experiment also shows the design is suitable for the decomposition of HAN solution as backflow successfully prevented. Qualitatively, relatively high *Re* and power required for decomposition of HAN solution to prevent formation of complex two-phase flow in the chamber.

A HAN-based micropropulsion system is currently being developed based on previous micro-combustion system design, by adding a nozzle to the chamber exit. Experiments and Quantitative analysis on various factors, such as packaging of microelectrodes, structural construction material and delivery of HAN solution are also being investigated to increase its efficiency. In addition, numerical studies will also be carried out to improve the engineering design. It is a challenging task as it involves parallel chemical reactions as well as complex liquid-gas two phase flow.

6. Acknowledgement

The authors would like to thank to Ministry of Science, Technology, and Innovation Malaysia (MOSTI) for funding the project (04-05-05-SF0008) through eScience Fund.

References

[1] R. H. Comer, Ignition and Combustion of Liquid Monopropellants at High Pressure, *Proc. 16th Int. Symp. On Combustion*, pp.1211-1219, 1976

[2] C. Kappenstein, N. Pillet, and A. Melchoir, Replacement of Hydrazine. The State of The Art, *Proc. 16-125, Intern. Conf. on Space Transportation for the XXI Century*. 2002

[3] T. G. Kang, S. W. Kim, and Y. H. Cho, High-Impulse, Low-power, Digital Microthrusters Using Low Boiling Temperature Liquid Propellant with High Viscosity Fluid Plug, *Sensors and Actuators A* , vol.97–98, pp659-664, 2002

[4] D. H. Lewis, S. W. Janson, R. B. Cohen, and E. K. Antonsson, Digital Micropropulsion, *Sensor and Actuators A*, vol.80, pp143–154, 2002

[5] D. Plumlee, J. Steciak, and A. Moll, Development and Simulation of an Embedded Hydrogen Peroxide Catalyst Chamber in Low-Temperature Co-Fired Ceramics, *Int. J. Appl. Ceram. Tech.*, vol.4, pp406–414, 2007

[6] M. H. Wu, and R. A. Yetter, A novel electrolytic ignition monopropellant microthruster based on low temperature co-fired ceramic tape technology, *Lab on Chip*, vol.9, pp910-916, 2009

[7] Y. G. Yu, M. Li, Y. H. Zhou, X. Lu, and Y. Z. Pan, Study on Electrical Ignition and Micro-explosion Properties of HAN-based Monopropellant Droplet, *Energy and Power Engineering in China*, Vol. 4(3), pp 430 – 435, 2010

[8] H. S. Chuang, and S. Wereley, Design, Fabrication and Characterization of a Conduction PDMS for Microheater and Temperature Sensors, *J. Micromech. Microeng.*, vol. 19, 045010, 2009

[9] H. S. Lee, A. L. Thomas, Chemical Kinetic Study of HAN Decomposition, *Combustion and Flame*, vol.135, pp151-169, 2003

[10] K. S. Koh, JK. Chin, T. F. Wahida, Role of Electrodes in Ambient Electrolytic Decomposition of Hydroxylammonium Nitrate (HAN) Solution, *J. Chem. Eng. Data*, (*Under Review*), 2013

[11] N. Nagai, M. Takeuchi, T. Kimura, T. Oka, Existence of Optimum Space Between Electrodes on Hydrogen Production of Water Electrolysis, *Int. J. Hydrogen Energy*, Vol 28, pp 35 – 41, 2003

[12] K. S. Koh, JK Chin, J. Chia, Quantitative Studies on PDMS-PDMS Interface Bonding with Piranha Solution and Its Swelling Effect, *Micromachines*, vol.3, pp.427-441, 2012